

## THE VELOCITY FIELD OF BRIGHT NEARBY GALAXIES. I. THE VARIATION OF MEAN ABSOLUTE MAGNITUDE WITH REDSHIFT FOR GALAXIES IN A MAGNITUDE-LIMITED SAMPLE<sup>1</sup>

ALLAN SANDAGE,<sup>2</sup> G. A. TAMMANN,<sup>3</sup> AND AMOS YAHIL<sup>4</sup>

Received 1978 October 23; accepted 1979 March 15

### ABSTRACT

The sample of all E and S0 galaxies in the magnitude-limited *Revised Shapley-Ames Catalog* (RSA) shows a strong and highly significant correlation of absolute magnitude with redshift. As an example, catalog galaxies with  $v_0 = 6000 \text{ km s}^{-1}$  are 2.6 mag brighter in  $M_B$ , in the mean, than galaxies with  $v_0 = 1000 \text{ km s}^{-1}$ . We show that this observed effect must exist in any magnitude-limited catalog of objects which have a broad luminosity function. In such a catalog, the concept of a fixed mean absolute magnitude (a standard candle) does not apply, and neglect of the variation of  $\langle M \rangle$  with  $v_0$  will cause photometric distances to be progressively incorrect with increasing redshift. Clearly, erroneous conclusions would be made concerning the linearity of the local Hubble expansion field if  $\langle M \rangle$  had been assumed to be constant.

In this paper we calculate the maximum likelihood distribution of  $M_B$  for E and S0 galaxies in the RSA [i.e., the luminosity function  $\varphi(M)$ ], and the completeness function  $f(m)$  of the catalog itself at various apparent magnitudes. We then show that the shapes of these distributions agree with the great cluster  $\varphi(M)$  function and with the direct data on the completeness of the RSA. The two calculated functions are then used to show that the *expected* variation of  $\langle M \rangle$  with  $v_0$  agrees with the *observed* correlation, provided that the underlying local velocity field is linear. No such agreement would have been obtained for a nonlinear velocity field, using the great cluster luminosity function.

We also show that the calculated luminosity functions for E and S0 galaxies differ significantly from each other. If the functions are normalized at  $M_{B_T} = -21$ , then the bright end of  $\varphi(M)$  for S0 galaxies is 0.7 mag fainter than for E systems. The wide scatter of the RSA E and S0 galaxies in the Hubble ( $m, v_0$ )-diagram is shown to be understood using the calculated  $\varphi(M)$  and  $f(m)$  distributions and a linear Hubble expansion. The slope of 5 in the Hubble  $m \sim 5 \log v_0$  equation, which is valid only if a particular sample of galaxies has a very narrow luminosity function, is, as expected, unrecognizable in these field galaxy data.

*Subject headings:* cosmology — galaxies: redshifts — luminosity function

### I. INTRODUCTION

The strongest observational evidence that redshifts increase linearly with distance for galaxies with redshifts larger than  $v_0 = 5000 \text{ km s}^{-1}$  (i.e., more remote than  $D \sim 100 \text{ Mpc}$ )<sup>5</sup> comes from data on the several brightest galaxies in individual clusters (Hubble and Humason 1931; Humason 1936; Hubble 1936; Humason, Mayall, and Sandage 1956), or more

recently from the first-ranked cluster galaxies themselves (Sandage 1972*b*). Additional evidence is provided by the inverse correlation of redshift and angular diameter, again for first-ranked cluster galaxies (Sandage 1972*a*), or, with larger scatter and hence less persuasion, by the angular diameter-redshift correlation for clusters themselves (Bahcall 1973; Hickson 1977; Bruzual and Spinrad 1978).

The first two proofs are powerful because *ratios* of distances can be obtained from observed intensity ratios with the high accuracy of  $\sigma(\delta r/r) \approx 15\%$  per cluster. This precision is due to the remarkably small dispersion of  $\sigma(M) \approx 0.3 \text{ mag}$  in the absolute magnitude of first-ranked cluster galaxies.

The mapping of the velocity field for very local galaxies (those with  $v_0 < 2500 \text{ km s}^{-1}$ ) is not nearly so simple because, except for Virgo and Fornax, no great clusters exist within the space, and the velocity-distance relation must be found using the bright field galaxies of low redshift. These galaxies, although numerous, have such a wide range of absolute luminosity that not only are the accuracies of photometric distances degraded, but unless special precautions are

<sup>1</sup> The order of names on the six expected papers of this series has been determined by a systematic permutation convention known only to the authors.

<sup>2</sup> Hale Observatories, Carnegie Institution of Washington. The Hale Observatories is operated jointly by the Carnegie Institution of Washington and the California Institute of Technology.

<sup>3</sup> Astronomisches Institut der Universität Basel, and European Southern Observatory.

<sup>4</sup> Astronomy Program, State University of New York, Stony Brook.

<sup>5</sup> In our notation  $v_0$  is the velocity of a galaxy corrected to the Sun and to the centroid of the Local Group, using the solar motion solution of Yahil, Tammann, and Sandage (1977). We use a Hubble constant of  $50 \text{ km s}^{-1} \text{ Mpc}^{-1}$  throughout this series of papers.

taken, systematic errors due to observational bias are easily introduced. Nonetheless, knowledge of the local flow is of quite fundamental importance because (1) a measurement of velocity perturbations caused by the large density contrast of the Virgo/Coma complex can give information about the universe as a whole (Sandage, Tammann, and Hardy 1972; Silk 1974; Peebles 1976), and (2) the solar motion relative to the mean flow of the nearby galaxies is important cosmologically.

Although the problem of the local velocity field has had a long past history, the results are still largely inconclusive. In contrast to claims of local linearity (Sandage and Tammann 1975; Sandage 1975), a large anisotropy has been suggested by de Vaucouleurs (1958, 1964, 1966, 1976), which he interprets as motion about the Virgo cluster. In a further study de Vaucouleurs (1972) suggests that these are superposed on a systematic *parabolic* expansion field (i.e.,  $v_0 \propto r^2$ ), which, however, is said to merge smoothly into a global linear Hubble flow ( $v_0 \propto r$ ) beyond  $v_0 \sim 6000 \text{ km s}^{-1}$ .

More radical is the conclusion of Hawkins (1962) and Segal (1975) from their separate analyses of the Hubble diagram for bright galaxies. They both suggest that even the *global* flow is parabolic at all distances, despite the evidence from the great clusters and the nearby groups.

Our present interest in the problem arose not in an effort to discuss these incompatible results, but rather in connection with a mapping of the local velocity field using galaxies with redshifts less than  $v_0 \sim 5000 \text{ km s}^{-1}$ , and in particular to determine the solar motion with respect to them. The sample is contained in the *Revised Shapley-Ames Catalog* (Sandage and Tammann 1979, hereafter RSA), for which velocities are now known for all but 12 of the 1246 entries. In order to determine the peculiar velocities of galaxies, we require photometric distances free from systematic errors caused by the broad luminosity function of the field galaxies. Otherwise, errors in distance that vary with redshift will be introduced, and no valid velocity field can be calculated.

We have found that this bias, caused by the severe variation of mean absolute magnitude of the galaxies in the sample with redshift, is the key both to the problem of the solar motion and to the local velocity field. This paper, the first in a series, is intended primarily as (1) a demonstration of the bias, (2) a discussion of methods for calculating it from the field luminosity function and the estimated incompleteness of the RSA, and (3) a comparison of the observed and the calculated variation of  $\langle M \rangle$  with  $v_0$ . The ultimate aim of the series is to search for velocity perturbations about the linear flow that arise from the density contrast of the Virgo complex. In Paper II we obtain the luminosity functions for spirals of different luminosity classes. These are needed for Paper III, where we treat the density structure of the local galaxies toward and away from Virgo and in other directions. The observed solar motion relative to the RSA and that expected from the density structures of Paper III are calculated in Paper IV, where comparison is made with the

motion suggested by Rubin *et al.* (1976) relative to slightly more distant galaxies, and by Smoot, Gorenstein, and Muller (1977), which they believe refers to the cosmic microwave background radiation. Paper V will treat the velocity field determined using the few galaxies whose distances are rather precisely known from their stellar content, and Paper VI will be a rediscussion of the Hubble constant using methods of the preceding papers.

In this paper certain technical matters important for the entire series are discussed. In § II we set out both the observed variation of  $\langle M \rangle$  with  $v_0$  and the Hubble diagram for E and S0 galaxies in the RSA. In §§ III and IV we give the calculation of the expected  $M$ ,  $v_0$  distribution for various field galaxy luminosity functions and for catalog completeness functions. In § V we compare our derived functions with external data. Finally, in § VI we compare these functions with the observations for catalog galaxies themselves in different redshift intervals.

## II. THE OBSERVED VARIATION OF ABSOLUTE MAGNITUDE WITH REDSHIFT

The RSA contains only the original Shapley-Ames galaxies. The catalog lists data on (1) types, (2) redshifts, (3) apparent  $B$  magnitudes reduced to the zero point of the *Second Reference Catalog* (de Vaucouleurs, de Vaucouleurs, and Corwin 1976), (4)  $B$  magnitudes corrected for galactic and internal absorption, and (5) corrected absolute magnitudes calculated from the redshifts using  $H_0 = 50 \text{ km s}^{-1} \text{ Mpc}$  as if the local expansion field were linear.

As shown in Figure 1, absolute magnitudes calculated in this way for E and S0 galaxies show a well-defined, large variation of  $M_B$  with redshift that ranges from  $M_B \sim -18$  to  $-23$  as the redshift increases from 400 to 7000  $\text{km s}^{-1}$ . In Figure 1 only the 255 E and S0 galaxies that are in the RSA are shown whose galactic latitudes are  $|b| \geq 30^\circ$ , and which are not in the Fornax cluster or within  $6^\circ$  of the center of the Virgo complex (taken as  $l = 280.4$ ,  $b = 74.6$ ). The region so defined is taken as our "standard sample" throughout this series. The plot for the more complete set of 325 E and S0 galaxies (still outside Virgo and Fornax), with no exclusion for galactic latitude, is similar, but the problem of what galactic absorption coefficient to use is largely avoided by the  $|b| > 30^\circ$  constraint.

A least-squares linear fit to the data of Figure 1 gives

$$M_B = -3.33(\pm 0.15) \log(v_0/10^3) - 19.83(\pm 0.06), \quad (1)$$

where  $v_0$  is in  $\text{km s}^{-1}$ . The variation of  $M$  with  $v_0$  is clearly significant.

To test the generality of the effect, solutions have been made with the sample subdivided into (a) the two galactic hemispheres, one of which is toward and the other away from the Virgo cluster, (b) galaxies with and without the galactic latitude exclusion, and (c) E and S0 types separately, with the results listed in Table 1. The solutions are the same to within statistics and show the stability of the correlation.

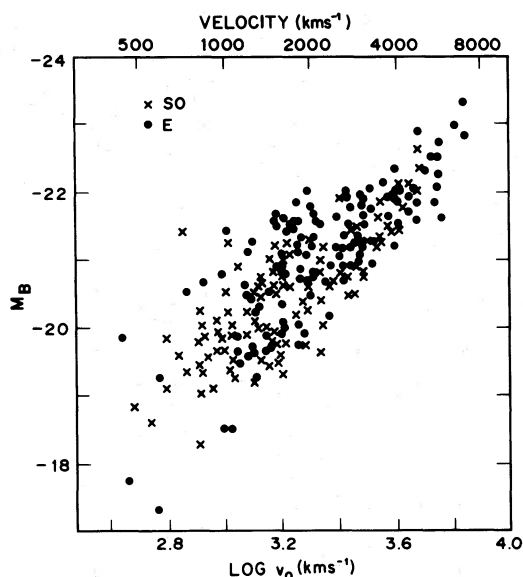


FIG. 1.—Variation of  $M_B$  with  $\log v_0$  for the standard sample of E and S0 galaxies (all galaxies with  $|b| > 30^\circ$ , excluding the Fornax cluster and  $6^\circ$  around the center of the Virgo cluster) from the magnitude-limited RSA catalog. The  $M_B$  values are calculated from  $v_0 = H_0 r$  using  $H_0 = 50 \text{ km s}^{-1} \text{ Mpc}^{-1}$ .

At first, two attitudes toward the magnitude-redshift relation might seem possible: (1) The most direct, but wrong, interpretation is that the calculated absolute magnitudes are incorrect because of the assumption of a linear velocity field. For example, if  $v_0 \propto r^n$ , then the absolute magnitudes calculated as if  $n = 1$  would be false, and a pseudo-variation of such

$M_B$  values with  $v_0$  would result. If the effect of a luminosity function of finite spread could be neglected, then clearly equation (1) would require that  $v_0 \propto r^3$ . It is this type of interpretation that has led Segal to the erroneous conclusion that  $n = 2$ . (2) The second possibility is that indeed  $v_0 \propto r$ ; that the  $M_B$  values calculated therefrom are correct (aside from small errors related to any random motions or a perturbed velocity field, to be discussed in Paper IV); and that the correlation is due to observational bias caused by a luminosity function that is broader than is encompassed by the apparent magnitude limit of the RSA. The purpose of the present paper is to develop this latter interpretation, and to show that with the known galactic luminosity function, the data in the RSA can be explained.

The observed effect is shown in a different representation in Figure 2, which is the redshift-apparent magnitude (Hubble) diagram for the standard sample of E and S0 galaxies. In this apparent magnitude-redshift plane, the linear regression of equation (1) transforms to

$$m_B = 1.67 \log v_0 + 6.67, \quad (2)$$

whose slope clearly differs from the canonical value 5, obtained when  $\langle M \rangle$  does not vary with  $v_0$ , i.e., if the galactic luminosity function would have been very narrow. One might ask why the problem of a bias in the Hubble relation could not be alleviated by a standard calculation of the classical Malmquist (1920) effect. A photometric distance can be obtained by a relation  $\log(r_{\text{ph}} \text{ Mpc}^{-1}) = 0.2(m - M_m - 25)$ , where  $M_m$  is the magnitude-limited mean luminosity. The advantage of this approach is that distances thus

TABLE 1  
LINEAR REGRESSION COEFFICIENTS OF ABSOLUTE MAGNITUDE-REDSHIFT RELATION FOR E AND S0 FIELD GALAXIES (Fornax and  $6^\circ$  around the Virgo center excluded)

CLASS (1)	SAMPLE (2)	n (3)	SLOPE (4)	$M_{B,3}^+$ (5)
E + S0	$ b  \geq 30^\circ$ *	255	$-3.33 \pm 0.15$	$-19.83 \pm 0.06$
	All	325	$-3.40 \pm 0.12$	$-19.83 \pm 0.05$
	$b > 30^\circ$	156	$-3.33 \pm 0.19$	$-19.81 \pm 0.06$
	$b < -30^\circ$	99	$-3.28 \pm 0.26$	$-19.88 \pm 0.11$
E	$ b  \geq 30^\circ$ *	134	$-3.26 \pm 0.21$	$-19.96 \pm 0.09$
	All	182	$-3.33 \pm 0.10$	$-19.96 \pm 0.04$
	$b > 30^\circ$	76	$-3.17 \pm 0.29$	$-19.98 \pm 0.12$
	$b < -30^\circ$	58	$-3.40 \pm 0.33$	$-19.92 \pm 0.15$
S0	$ b  \geq 30^\circ$ *	121	$-3.13 \pm 0.21$	$-19.75 \pm 0.07$
	All	143	$-3.18 \pm 0.14$	$-19.75 \pm 0.05$
	$b > 30^\circ$	80	$-3.24 \pm 0.24$	$-19.71 \pm 0.07$
	$b < -30^\circ$	41	$-2.87 \pm 0.43$	$-19.87 \pm 0.16$

\*The "standard sample"

+Absolute magnitude from equation (1) of the text at  $v_0 = 1000 \text{ km s}^{-1}$ .

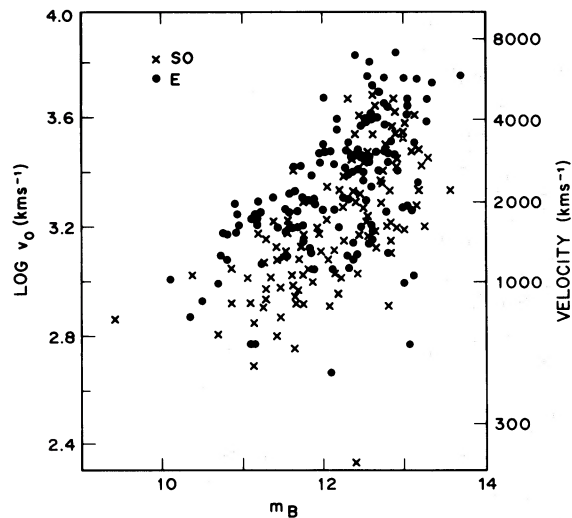


FIG. 2.—The Hubble diagram ( $\log v_0$  versus apparent blue magnitude) for the same galaxies shown in Fig. 1.

obtained are free from the apparent magnitude selection function. However, the classical Malmquist calculation cannot simply be applied to our problem. The Malmquist bias, i.e., the difference  $\Delta M = M_d - M_m$  between the true (distance-limited) and the magnitude-limited mean luminosities, depends on the variation of the number density with distance (e.g., the bias  $\Delta M = 1.38 \sigma^2$  for a Gaussian luminosity function holds only if  $dN \propto v^2 dv$ ). The large density fluctuations within the volume spanned by the RSA galaxies will change this bias from region to region, and from one range of apparent magnitude to another, making photometric distances both density-dependent and difficult to interpret.

However, the problem can be studied in a way that, in certain of its aspects, does not depend on the density structure of the local neighborhood. With this in mind, our approach has been to abandon the traditional calculation of the Malmquist bias, and instead, to approach the problem of bias-free photometric distances by means of the correlations of equation (2), applied here to E and S0 galaxies, and applied in Papers II and III to spirals of different luminosity classes. In doing so we have proceeded by determining the systematic variation of absolute magnitude with redshift for galaxies in the RSA, and show here that it can be calculated from the luminosity function and the catalog completeness function, independent of any density fluctuations. The method is therefore suitable for the study of peculiar velocities brought about by those density variations.

### III. UPPER AND LOWER ENVELOPES

One can understand the distributions in Figures 1 and 2 on at least three levels. The simplest is a calculation of the upper and lower boundary lines. This requires only minimal use of the data and of the adopted distribution functions. Somewhat more detailed is a calculation of the *mean* correlation

between  $M_B$  and  $v_0$  (eq. [1]), which depends only on an integration using the adopted distribution functions. Most stringent is a comparison of the *entire observed distribution* of  $M_B$  at any redshift with that expected from optimized luminosity and catalog completeness functions; this calculation clearly depends on the details of the functions themselves. We have made all three comparisons and describe them in this and the following sections.

The upper and lower envelopes of the  $(M_B, v_0)$  distribution in Figure 1 can be calculated using any given field luminosity function, provided that the catalog completeness is known. The most directly calculated lower boundary is that obtained by assuming that the RSA is sharply terminated for galaxies fainter than  $B = 13.2$ , and that there are enough galaxies in each redshift interval to provide at least one listing at this limit. This lower bound is shown as the solid straight line in Figure 3 whose equation is  $B = 13.2$ , or  $M_B(\text{lower}) = -3.31 - 5 \log v_0$  in the  $(M_B, v_0)$ -plane.

The somewhat brighter curved thin line in Figure 3 is a different lower bound, calculated using the catalog completeness function derived in the next section that describes the fraction of the total sample detected in the RSA at each apparent magnitude.

The upper bound is that line above which one galaxy, on the average, will appear in the volume enclosed within a given redshift  $v_0$ . (The lower limit mentioned in the last paragraph is analogously defined.) Clearly, the *shape* of this bound depends only on the *form* of the assumed luminosity function, provided that the catalog is complete at the appropriate apparent magnitudes. Its position depends on the normalization of the luminosity function (i.e., on the number of galaxies per unit volume brighter than  $M$ ; in the present discussion we ignore density inhomogeneities, as it can be shown that the density contrasts determined in Paper III have only a small effect on the upper envelope line).

Let  $\Phi(M)$  be this integral luminosity function. The number of galaxies brighter than  $M$  in the volume out to redshift  $v_0$  and within a solid angle of  $\Omega$  sr is clearly

$$N(v_0) = \Omega/3(v_0/H_0)^3 \Phi(M), \quad (3)$$

where  $v_0$  is in  $\text{km s}^{-1}$ ,  $H_0$  is in  $\text{km s}^{-1} \text{Mpc}^{-1}$ , and  $\Phi(M)$  is the number of galaxies per cubic Mpc brighter than  $M$ .

The upper envelope can be calculated explicitly from (3) by setting  $N(v_0) = 1$ . As an example, we can suppose that the field luminosity function has the same shape as that for the great clusters (e.g., Abell 1975), and test the consequences. The cluster data can be fitted by various functions, one of which is

$$\log [\Phi(M)/K] = \frac{A - M}{B - \alpha M}, \quad (4)$$

where  $K$  defines the normalization, and  $A$ ,  $B$ , and  $\alpha$  are constants.

It is known that this form represents the cluster data with good accuracy over intervals greater than 6 mag

in  $M_V$  and four decades in  $\Phi(M_V)$  (Sandage 1976, Fig. 4), when  $A_V = -20.067$ ,  $B_V = -10.202$ , and  $\alpha_V = +0.384$ . The conversion from  $M_V$  to  $M_B$  is adequately accomplished by assuming  $M_B = M_V + 0.8$  in the mean for E and S0 galaxies over the relevant range of absolute luminosities. This transformation requires  $A_B = -19.267$ ,  $B_B = -9.895$ , and  $\alpha_B = +0.384$ .

The normalization  $K$  has been determined for E and S0 galaxies by requiring (4) to give the total number of such galaxies in the RSA, after the catalog is corrected for incompleteness as described in the next section. With this normalization, which is an average over the density contrasts in the regions occupied by the standard sample of E and S0 galaxies in RSA (with the Fornax Cluster and a  $6^\circ$  radius about the Virgo Cluster removed), the integral luminosity function is

$$\log \Phi(M_B) = \frac{-19.267 - M_B}{-9.895 - 0.384 M_B} - 2.89$$

$$\equiv \{ \} - 2.89, \quad (5)$$

where the brackets represent the right side of (4). The units of  $\Phi(M_B)$  in (5) are the number of E plus S0 galaxies per cubic Mpc brighter than  $M_B$ .

Substituting (5) into (3) and setting  $\Omega = 2\pi$  to account for the fraction of the sky that is unsampled due to the  $|b| \geq 30^\circ$  restriction (the  $6^\circ$  around Virgo modify this fraction by only 0.5%) gives an equation for the upper envelope as

$$3 \log v_0 = -\{ \} + 7.67, \quad (6)$$

and because the quantity in brackets is a function of  $M_B$  alone, equation (6) defines the locus  $N(v_0) = 1$  in the  $(M_B, v_0)$ -plane. Equation (6) is a good fit to the distribution of the brightest points at various redshifts in Figure 1. Note that the normalization constant of 7.67 was fixed independently of the  $M_B, v_0$  distribution itself, yet equation (6) does describe the upper envelope well.

The envelope line actually shown in Figure 3 is not equation (6) but is everywhere closer than  $\Delta M_B \sim 0.3$  mag to it for  $M_B$  brighter than  $-19$ . The line that is drawn was calculated by the method just described, but we used our final maximum likelihood luminosity function described in the next section, rather than equation (5). We later show (see Fig. 5) that this finally optimized function is almost the same as the great cluster function (eq. [5]). Hence the same general luminosity function approximates both the clusters and the general field—not a new finding (cf. Christensen 1975).

Two final points should be made concerning this simplified calculation. (1) It is clear why the upper envelope slopes toward fainter magnitudes at small redshifts. The sample volume is so small for low  $v_0$  that only intrinsically faint galaxies exist within it because the probability of finding brighter galaxies is low (i.e., the luminosity function is very steep at the bright end). (2) The calculation given here is for constant density everywhere, and hence neglects variations of density

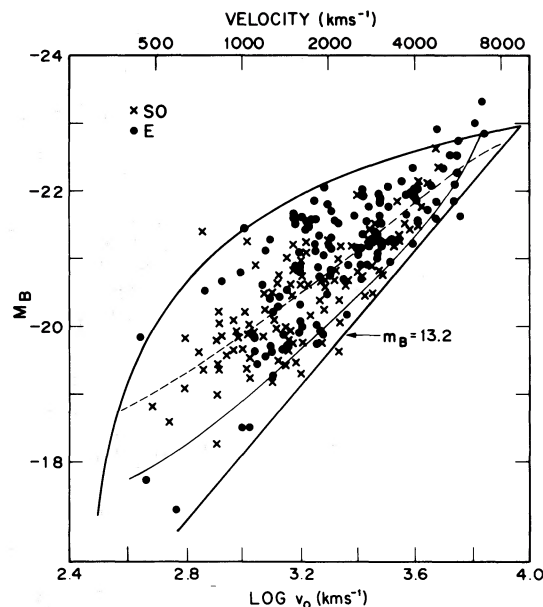


FIG. 3.—Same as Fig. 1 but with upper and lower envelope lines and the calculated mean  $\langle M \rangle$  versus  $\log v_0$  line drawn. Two lower envelope boundary lines are shown. The heavy solid line is for a sharp catalog limit of  $B = 13.2$ . The lighter curved boundary is the locus of  $N(\text{faintest}) = 1$  when the completeness function of eq. (8) is used. Shown as a dashed line is the mean absolute magnitude calculated from eq. (7), using the optimized luminosity and completeness functions.

with distance. For the nonhomogeneous but spherically symmetric case, the right-hand side of equation (3) contains a density factor  $D(v_0)$ . But as previously mentioned, the main features of this more realistic case, where  $D(v_0)$  varies by factors of  $< 4$  from the mean, differ only slightly from the upper envelope in the log-log plot of Figure 3.

#### IV. MAXIMUM LIKELIHOOD LUMINOSITY AND COMPLETENESS FUNCTIONS

If the luminosity function in (5) is correct, and if the RSA were complete to a given apparent magnitude, then the calculated mean absolute magnitude of the sample at any redshift should closely approximate the observed  $\langle M \rangle, v_0$  correlation of (1). The mean absolute magnitude at a given  $v_0$  can be calculated by progressively terminating the luminosity function at its faint end at the absolute magnitude  $M_L(v_0)$ , which corresponds to the apparent magnitude limit of the catalog (i.e., the lower envelope line in Fig. 3). Clearly  $M_L$  is a function of  $v_0$  given by

$$M_L = 13.2 - 5 \log(v_0/H_0) - 25$$

if the catalog limit is taken as  $m = 13.2$ . If  $\varphi(M)$  is the differential luminosity function, found directly from the integral function  $\Phi$  by differentiation, and  $D(v_0)$  is the mean density factor, then the mean absolute magnitude at redshift  $v_0$  is

$$\langle M_B \rangle(v_0) = \frac{\int_{-\infty}^{M_L(v_0)} M D(v_0) \varphi(M) dM}{\int_{-\infty}^{M_L(v_0)} D(v_0) \varphi(M) dM}. \quad (7)$$

An important point, which is obvious intuitively but shown explicitly by (7), is that  $\langle M \rangle$  at any given  $v_0$  is independent of the density as long as  $\varphi(M)$  and  $D(v)$  are not coupled;  $D(v)$  cancels in the numerator and the denominator of (7). (We ignore the second-order Eddington correction discussed by Schechter 1976.)

Equation (7) has a simple meaning. Consider a vertical line in Figure 1 and determine the mean of the distribution of points along it, given that the population density increases faintward by the probability distribution  $\varphi(M)$ . Because the catalog limit slopes downward in Figure 3,  $\langle M \rangle$  must also become fainter for small redshifts, as observed, provided that  $\varphi(M)$  is broad enough.

In a trial calculation using the differential of (5) in (7), however, we obtained a predicted variation of  $\langle M \rangle$  with  $v_0$  much steeper than is observed (eq. [1]). This can only mean that the increase of galaxies in the RSA is *less steep* than given by  $\varphi(M)$  alone, as the lower boundary in Figure 1 is approached. We are not permitted to change the shape of  $\varphi(M)$ , as that is fixed by the upper envelope fit. Rather, the cause is a progressive incompleteness in the Shapley-Ames catalog as its limiting apparent magnitude is approached. This is not surprising, of course, since the catalog incompleteness has been known from independent data (see de Vaucouleurs 1956).

The parameters of some appropriate completeness function  $f(m)$  could be determined by requiring that the  $\langle M \rangle, v_0$  relation calculated from (7) agree with (1), when  $\varphi(M)$  is replaced by  $\varphi(M)f(m)$  at every  $v_0$ . [Recall that  $M$  and  $m$  are related by  $m = M + 5 \log(v_0/H_0) + 25$ .] However, the most efficient way to determine  $f(m)$  is to optimize the coefficients in given functional forms of  $\varphi(M)$  and  $f(m)$  so as to satisfy the *entire distribution* of points in Figure 1, i.e., to obtain the maximum likelihood estimates (see Jauncey 1967, or a standard statistics reference, such as Kendall and Stuart 1973).

Suppose there are  $n$  coefficients to be optimized in the  $\varphi(M)f(m)$  product. It is clearly advantageous that  $n$  be as small as possible because the sharpness of the convergence depends on  $n$  as each coefficient is varied in the calculations that locate the highest peak in the  $n$ -dimensional parameter space that defines the probability density [i.e., the product of the individual probabilities of finding data points at their absolute magnitudes in Figure 1, given adjustable  $\varphi(M)$  and  $f(m)$  distributions; cf. eq. (10) described later]. Hence, to calculate the optimal  $\varphi(M)$  and  $f(m)$  functions, we have not used equation (4), which has three parameters to vary, but rather choose the  $\varphi(M)$  form suggested by Schechter (1976), which has only two. (Note that the normalization constants in equation (4) and in the Schechter function need not be optimized as they are fixed by the number of catalog entries, corrected by the completeness function.) The parameters to be determined are the absolute magnitude  $M_0$  corresponding to Schechter's  $L^*$  (not to be confused with Abell's  $M^*$  which does not exist in representations where the integral luminosity function has a continuous first derivation everywhere) and  $\beta$ , which is the slope of

$\varphi(M)$  at faint  $M$  (equal to  $\alpha + 1$  in Schechter's notation).

We take the form of the completeness function from the Fermi-Dirac distribution function as

$$f(m) = \{\exp [(m - m_L)/\Delta m_L] + 1\}^{-1}, \quad (8)$$

where  $f(m)$  is the fraction of the total sample that is listed in the catalog at any  $m$ , and where  $m_L$  and  $\Delta m_L$  are the parameters to be determined.

The maximum likelihood method finds the best values of  $M_0, \beta, m_L,$  and  $\Delta m_L$  by varying each until the product of the individual probability-densities of the data sample reaches its maximum value. It is important to note, as we now explicitly show here, that this method of calculating  $\varphi(M)$  and  $f(m)$  is independent of any density fluctuations, and further, is a "continuum" calculation; it requires no binning of the data.

Let  $P(M, v_0)$  be the probability that a galaxy whose observed redshift is  $v_0$  will have an absolute magnitude brighter than  $M$ . To visualize the problem, consider the distribution of points in Figure 1 and ask of any given galaxy  $i$  at  $M_i, v_{0,i}$  what is the probability that a random catalog galaxy at the same redshift will be brighter than  $M_i$ . At any given  $v_0$ , the apparent magnitude corresponding to a particular absolute magnitude  $M$  is  $m = M + 5 \log(v_0/H_0) + 25$  as before. Hence, at any given  $v_0$  the completeness function  $f(m)$  is known at every point along a vertical line in Figure 1. Clearly the required probability is

$$P(M, v_0) = \frac{\int_{-\infty}^M \varphi(M') D(v_0) f(m') dM'}{\int_{-\infty}^{+\infty} \varphi(M') D(v_0) f(m') dM'}, \quad (9)$$

which can be calculated for any observed  $M, v_0$  pair once the four parameters in  $\varphi(M)$  and  $f(m)$  are known. Since  $D(v_0)$  is not a function of  $M$ , it can be taken outside the integral in both numerator and denominator, and it cancels, which was to be shown. The probability  $P(M, v_0)$  depends only on the parameters  $M_0, \beta, m_L,$  and  $\Delta m_L$ .

This cumulative probability  $P(M, v_0)$  has associated with it a differential probability density  $p(M, v_0) = \partial P(M, v_0)/\partial M$ . The maximum likelihood technique is the search for the individual values of the parameters  $M_0, \beta, m_L,$  and  $\Delta m_L$  which maximize the product  $L$  of the probability densities taken at all the data points of the sample, i.e.,

$$L = \prod_i p(M_i, v_{0,i}), \quad (10)$$

which itself depends only on the four parameters which we wish to optimize.

We used a routine developed for problems in high-energy physics, which is available as a standard program in the computer library, to maximize  $L$  in the four-dimensional parameter space. Standard search routines are available to test if the resulting maximum is a global maximum or only a local maximum. Furthermore, the sharpness of the maxima in  $L$  as each parameter is varied is a measure of the accuracy to

TABLE 2  
MAXIMUM LIKELIHOOD COEFFICIENTS FOR THE INTEGRAL LUMINOSITY  
AND CATALOG COMPLETENESS FUNCTIONS

CLASS	SAMPLE	$\phi$ ( $M_B$ )		$f(m)$		
		$M_0$	$\beta$	$m_L$ (B)	$\Delta m_L$ (B)	
a) Schechter Function Assumed						
E + SO	$ b  > 30^\circ$	$-20.80 \pm 0.11$	$+0.08 \pm 0.21$	$12.83 \pm 0.10$	$0.16 \pm 0.02$	
	$b > 30^\circ$	$-20.75 \pm 0.11$	$+0.07 \pm 0.11$	$12.84 \pm 0.10$	$0.16 \pm 0.01$	
	$b < -30^\circ$	$-20.93 \pm 0.10$	$+0.08 \pm 0.36$	$12.84 \pm 0.19$	$0.16 \pm 0.07$	
	All	$-20.96 \pm 0.10$	$-0.12 \pm 0.18$	$12.73 \pm 0.10$	$0.18 \pm 0.01$	
	$\left\{ \begin{array}{l} b > 30^\circ \\ b < -30^\circ \end{array} \right\}^\dagger$		$-20.75 \pm 0.13$	$0.06 \pm 0.23$	$\{12.83 \pm 0.13$	$0.16 \pm 0.02\}^\dagger$
			$-20.84 \pm 0.16$	$0.17 \pm 0.21$		
E	$ b  > 30^\circ$	$-20.93 \pm 0.10$	$0.22 \pm 0.28$	$12.80 \pm 0.13$	$0.16 \pm 0.02$	
	$b > 30^\circ$	$-20.98 \pm 0.10$	$0.30 \pm 0.10$	$12.96 \pm 0.10$	$0.14 \pm 0.02$	
	$b < -30^\circ$	$-20.96 \pm 0.10$	$-0.05 \pm 0.18$	$12.63 \pm 0.10$	$0.17 \pm 0.02$	
	All	$-20.96 \pm 0.10$	$+0.12 \pm 0.10$	$12.70 \pm 0.10$	$0.18 \pm 0.02$	
	$\left\{ \begin{array}{l} b > 30^\circ \\ b < -30^\circ \end{array} \right\}^\dagger$		$-20.94 \pm 0.10$	$+0.16 \pm 0.10$	$\{12.80 \pm 0.10$	$0.17 \pm 0.02\}^\dagger$
			$-20.87 \pm 0.10$	$+0.41 \pm 0.10$		
SO	$ b  > 30^\circ$	$-20.14 \pm 0.20$	$+0.44 \pm 0.34$	$12.86 \pm 0.22$	$0.16 \pm 0.04$	
	$b > 30^\circ$	$-19.91 \pm 0.32$	$+0.02 \pm 0.64$	$12.41 \pm 0.24$	$0.21 \pm 0.04$	
	$b < -30^\circ$	$-20.50 \pm 0.52$	$+0.38 \pm 0.43$	$13.03 \pm 0.20$	$0.12 \pm 0.04$	
	All	$-20.21 \pm 0.35$	$+0.23 \pm 0.37$	$12.74 \pm 0.20$	$0.18 \pm 0.04$	
	$\left\{ \begin{array}{l} b > 30^\circ \\ b < -30^\circ \end{array} \right\}^\dagger$		$-19.99 \pm 0.21$	$+0.53 \pm 0.34$	$12.87 \pm 0.21$	$\{0.15 \pm 0.04\}^\dagger$
			$-20.38 \pm 0.18$	$+0.37 \pm 0.40$		
b) Great Cluster Function (Equation 4)						
E + SO	$ b  > 30^\circ$	$A_B = -19.267;$		$12.72 \pm 0.06$	$+0.19 \pm 0.01$	
	All	$B_B = -9.985; \alpha = +0.384$		$12.67 \pm 0.01$	$+0.19 \pm 0.02$	

$^\dagger$ The coefficients of the completeness function are forced to be identical in these two samples so as to test the similarity of  $\phi(M)$  in the north and south galactic hemispheres separately.

which that given parameter is determined. Our estimates of the associated mean errors are derived from the second derivatives of  $L$  at its maximum, and are based on the asymptotic normality of the maximum likelihood estimators (Kendall and Stuart 1973). The errors are formal, and although they should not be overinterpreted, they do give some idea of the accuracies of the individual parameters.

The optimal values of the four coefficients found in this way are listed in Table 2, using the same division of the data as in Table 1. Also listed are the maximum likelihood values of  $m_L$  and  $\Delta m_L$  when  $\phi(M)$  is fixed to be the great cluster function [i.e., eq. (4) for the integral representation, or its derivative for  $\phi(M)$ ]. In addition, the data have been divided into the north and south galactic hemispheres, with fixed  $m_L$  and  $\Delta m_L$  to test if the shape of  $\phi(M)$  differs in what are essentially directions toward and away from the Virgo/Coma complex; no significant difference is found.

Inspection of Table 2 shows that the optimized func-

tions are very stable for nearly all of the subsets of the data sample, and in particular for divisions into the galactic hemispheres, and for inclusion or exclusion of the galactic zone of avoidance. Furthermore, fixing the luminosity function to be equation (5) gives an  $f(m)$  function that is nearly the same as that obtained from the cases where  $\phi(M)$  is also allowed to vary (i.e., the optimized Schechter function).

We now return to the calculation of mean absolute magnitude as a function of redshift using the optimized  $\phi(M)$  and  $f(m)$  distributions. Consider the standard sample of Figure 1 (i.e., the entire sky, but with  $|b| < 30^\circ$ , the Fornax Cluster and the  $6^\circ$  radius about the Virgo cluster excluded) and the  $\phi(M)$  and  $f(m)$  functions that apply to it from Table 2. Replacing equation (7) by

$$\langle M_B \rangle = \frac{\int_{-\infty}^{+\infty} M \phi(M) f(m) dM}{\int_{-\infty}^{+\infty} \phi(M) f(m) dM} \quad (11)$$

gives the  $\langle M \rangle, v_0$  relation shown as a dashed line between the upper and lower boundary lines in Figure 3. Between  $M_B \approx -18.5$  and  $-23$  this mean line is nearly linear with an equation

$$\langle M_B \rangle = -3.05 \log(v_0/10^3) - 19.92, \quad (12)$$

for comparison with equation (1). Clearly the agreement between (1) and (12) is excellent, which was to be proved. Stated differently, *a basic underlying linear-expansion velocity field appears to be highly nonlinear in the observed data of redshift and apparent magnitude, when mapped using field galaxies of widely different absolute magnitudes that have been taken from a catalog that is limited in apparent magnitude.*

This, our main conclusion, is shown explicitly in the Hubble diagram of Figure 4, which is the same as

Figure 2, except that the upper and lower envelope lines and the mean line of Figure 3 are shown. An ideal Hubble line of  $m_B = 5 \log v_0 + \text{constant}$  is unrecognizable.

We now examine the problem more closely by testing whether the optimized  $\varphi(M)$  and  $f(m)$  functions of Table 2 that reproduce the observed  $\langle M \rangle, v_0$  relation are, in fact, reasonable by comparing them with independently known external data.

#### V. COMPARISON OF THE OPTIMIZED $\varphi(M)$ AND $f(m)$ FUNCTIONS WITH EXTERNAL DATA

##### a) The Luminosity Function

There is increasing evidence that the luminosity function for field galaxies is the same as that for the

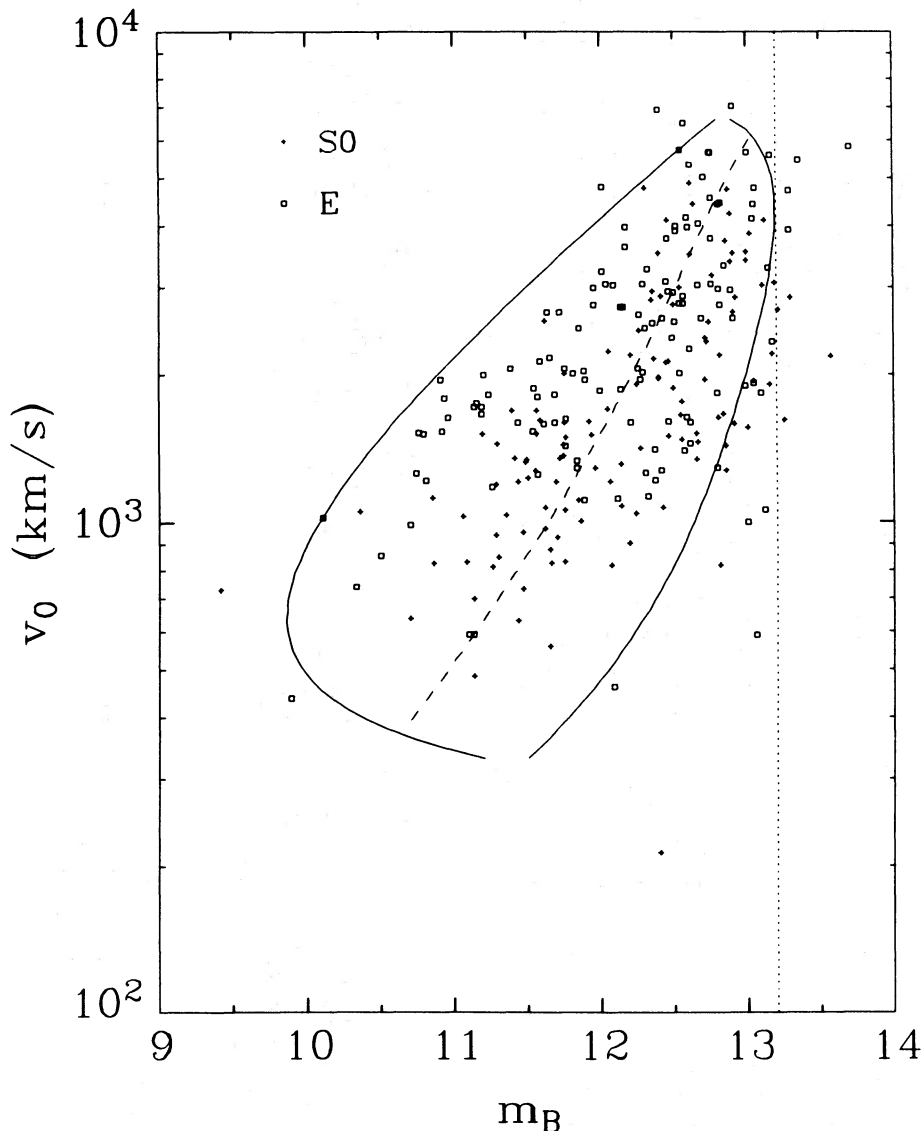


FIG. 4.—The Hubble diagram as in Fig. 2 but showing the upper and lower envelope lines and the mean lines of Fig. 3. A linear approximation to the dashed mean line is  $m_B \approx 1.95 \log v_0 + 5.73$  which is a much weaker dependence of  $m$  on  $v$  than the  $5 \log v_0$  that would apply if the luminosity function were infinitely narrow.

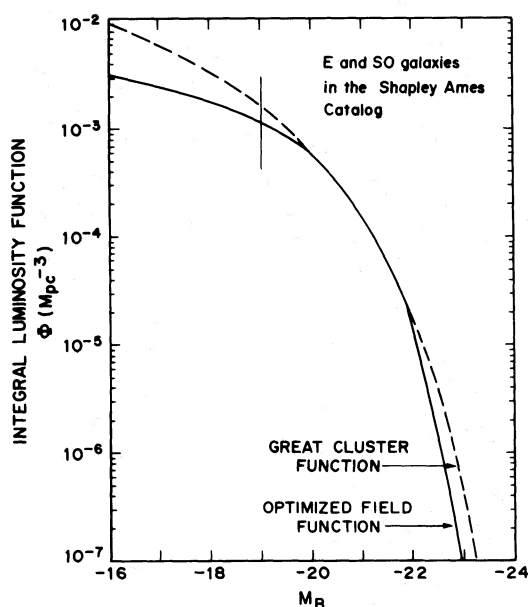


FIG. 5.—Comparison of the integrated luminosity function of the great clusters (*dashed line*) from eq. (4), and the optimized function for the standard sample of field E and S0 galaxies in the RSA (*solid line*). The functions are normalized to the total number in the catalog, corrected for incompleteness. The unit is number of E and S0 galaxies brighter than  $M_B$  per cubic Mpc.

great clusters (cf. Christensen 1975). Hence a comparison of the optimized two-parameter Schechter function with the cluster equation (4) is a test of the reality of our separate determinations of the individual  $\varphi(M)$  and  $f(m)$  functions themselves, as in Table 2.

The comparison is made in Figure 5 which shows the integrated luminosity function of E and S0 cluster galaxies as a dashed line, compared with the field function which was optimized using the standard sample.

It is to be noted from Figure 1 (but more explicitly from Fig. 11 discussed later) that the sensitivity of our data for  $M_B$  fainter than  $\sim -19$  is almost nil because there are so few galaxies, and hence no real information

is present in Figure 5 leftward of the vertical line drawn at this magnitude. With this disclaimer, the observed and the optimized hypothetical functions are excellent fits. The deviations are only in detail, and we believe they cannot be considered as suggesting a real difference between the functions. This agreement is encouraging as it shows that our adopted  $\Phi(M)$  is realistic.

#### b) The Completeness Function

The reality of the completeness function can be tested by comparing equation (8) with an external count of the number of galaxies that should be in the Shapley-Ames but are not. A list of  $\sim 800$  such galaxies has been prepared from all available sources, as discussed in the preface to the RSA. The known catalog additions are nearly complete for  $\delta > -3^\circ$  (i.e., the declination limit of the Zwicky *et al.* catalog), and we make the comparison for those E and S0 galaxies in the standard sample that are north of  $-3^\circ$  declination.

The data, listed in Table 3, are illustrated in Figure 6. Column (2) shows the number actually listed in the RSA; column (3) is the number of E and S0 galaxies known from the list of 800 new candidates; columns (6) and (7) are the *predicted* completeness ratios using equation (8) and the optimized parameters of Table 2. The agreement between our formalism and the actual incompleteness is excellent. In this regard it should be emphasized that the data and the formalism are entirely independent; the observations were not used in the optimization process, and were not, in fact, known until the values in Table 2 were complete. Hence, the agreement is highly significant, showing that the machinery developed here is not merely formal but is *required by the external data* for both  $\Phi(M)$  and  $f(m)$ . In this sense, the variation of  $\langle M \rangle$  with  $v_0$  in § II can be said to be understood.

#### VI. DETAILED DISTRIBUTION OF $M_B$ VALUES AT GIVEN REDSHIFTS

The most detailed test of how well all the data have been described by the assumed  $\varphi(M)$  and  $f(m)$  func-

TABLE 3  
COMPARISON OF PREDICTED AND OBSERVED COMPLETENESS FUNCTION FOR E AND S0 GALAXIES IN THE REGION  $\delta > -3^\circ$  AND  $|b| \geq 30^\circ$

$m_B$ (1)	Number Listed (2)	Number Not Listed (3)	Total Number (4)	Fraction Detected (5)	$f(m)$ Field (6)	$f(m)$ Cluster (7)
11.95 - 12.14	10	0	10	1.00	0.99	0.97
12.15 - 12.34	16	1	17	0.94	0.97	0.92
12.35 - 12.54	12	4	16	0.75	0.91	0.81
12.55 - 12.74	12	6	18	0.67	0.75	0.59
12.75 - 12.94	11	20	31	0.35	0.47	0.34
12.95 - 13.14	11	25	36	0.31	0.20	0.15
13.15 - 13.34	4	33	37	0.11	0.07	0.06
13.35 - 13.40	(1)	(11)	(12)	(0.08)	0.03	0.03

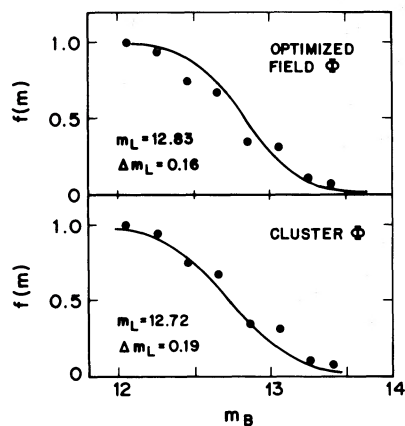


FIG. 6.—Comparison of the observations with the theoretical completeness function as optimized using the best Schechter function (*top panel*) or the great cluster function of eq. (4) (*bottom panel*) for E and S0 galaxies only. The data are from Table 3 and include only galaxies with  $\delta > -3^\circ$ ,  $|b| > 30^\circ$ .

tions is a comparison of the observed probability distribution of absolute magnitude at specific redshifts with that expected from theory. As before (eq. [9]), let  $P(M, v_0)$  be the probability that a galaxy observed to have redshift  $v_0$  will have absolute magnitude brighter than  $M$ .

If the assumed  $\varphi(M)$  and  $f(m)$  adequately describe the data, then the set of calculated probabilities  $P(M, v_0)$  of all the galaxies using their absolute magnitudes  $M$  and velocities  $v_0$  in equation (9) should be homogeneously distributed between 0 and 1. Furthermore, the probability values should not be correlated with  $v_0$ , and a homogeneous distribution should be obtained in any redshift interval.

The distribution of calculated probabilities  $P(M, v_0)$  of the galaxies in our standard sample is shown in Figure 7. The entire sample is shown in the upper right panel, and subsamples of redshift intervals are shown in the other panels. The Poisson  $N^{1/2}$  errors are shown as vertical bars, and the distributions are seen to be homogeneous, within statistics.

A different representation of the same test is to compare the *observed distribution of absolute magnitudes* with that calculated from the adopted  $\varphi(M)$  and  $f(m)$  functions in appropriate velocity intervals. Although straightforward, it is convenient to visualize the calculation by reference to Figure 1. Consider a velocity interval centered at some  $v_0$ , of width  $\Delta v_0$ , and look at the distribution in  $M_B$  of the observed points within that strip. The differential luminosity function  $\varphi(M)$  would give the expected distribution were it not for the catalog incompleteness. Lines of constant apparent magnitude  $m_B$  are parallel to the solid lower envelope in Figure 3, and these define the loci of constant  $f(m)$ . Hence, everywhere in a particular vertical strip,  $f(m)$  and  $\varphi(M)$  are known, and the expected distribution in  $M_B$  may be calculated. The finite width of the strip does introduce a slight dependence on the density function  $D(v_0)$  near the faint end, because the argument of the completeness function  $f(m)$  is the ap-

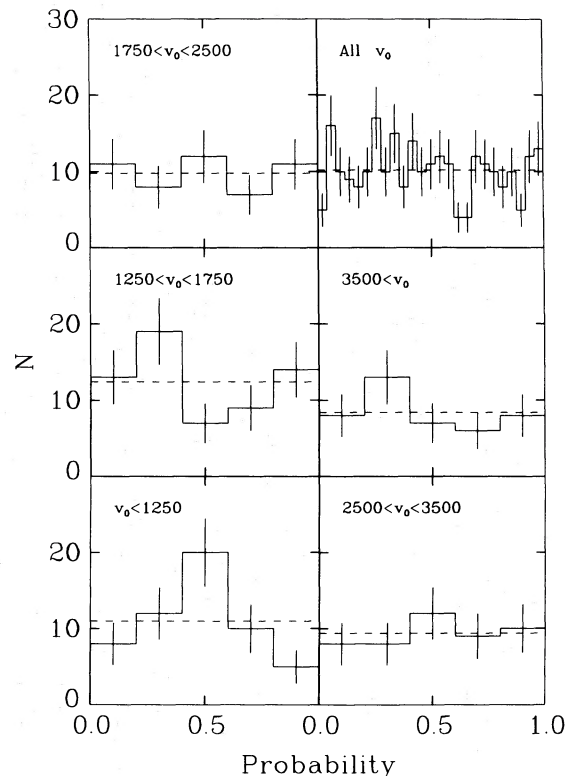


FIG. 7.—Histograms of the calculated probability of finding a galaxy that is actually found to be brighter (in  $M_B$ ) than any given E and S0 galaxy in the standard sample of the RSA whose absolute magnitude is itself  $M_B$ . The probabilities are calculated for every galaxy in the sample, using the optimized  $\varphi(M)$  and  $f(m)$  functions in eq. (9). They are separated into five velocity intervals and binned in probability intervals of 0.2. The dashed line in each panel is the expectation value for a uniform distribution of probabilities which would apply if the luminosity and completeness functions fitted the data exactly. Data from all velocity intervals are combined in the upper right panel. Vertical lines in each histogram are the  $N^{1/2}$  errors of each entry.

parent and not the absolute magnitude, but the effect is small.

Figure 8 shows the observed distributions within the five velocity intervals, together with the calculated expectations, using the optimized functions. In calculating the expected distribution, the density function  $D(v_0)$  was assumed to be constant within each small velocity interval, but allowed to vary from interval to interval. The normalization is such that the area under each curve is equal to the total number of galaxies actually observed in that interval. The systematic variation of  $\langle M_B \rangle$  with  $v_0$  is clearly evident; there is a progressive leftward shift as the mean velocity decreases. The model shows that  $\langle M_B \rangle$  varies from  $-22.0$  to  $-19.8$  as the velocities decrease from  $v_0 > 3500 \text{ km s}^{-1}$  to  $< 1250 \text{ km s}^{-1}$ . Note also the change of  $\sigma(M_B)$  with velocity—shown observationally in Figure 1 as the change in the spread in the points with  $v_0$ , and reproduced by the model as shown by the increased width of the continuous curves as  $v_0$  decreases

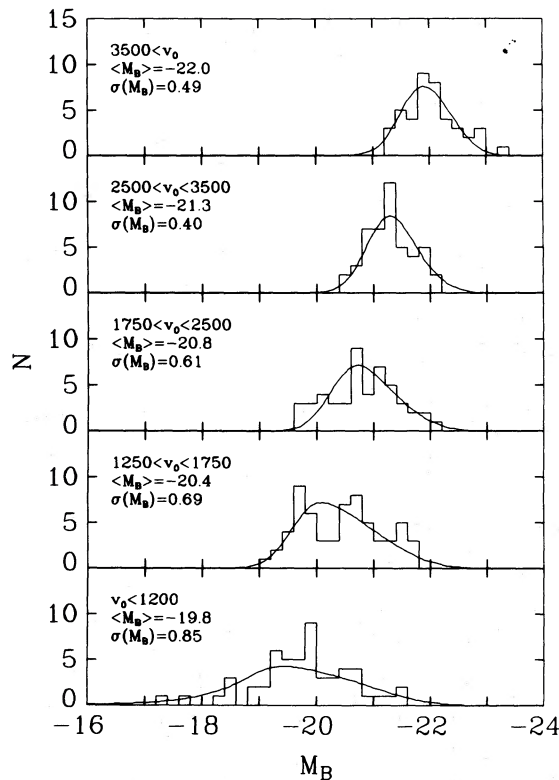


FIG. 8.—Histograms of the observed distribution of  $M_B$  for the E and S0 galaxies in the standard sample, separated into five velocity intervals and binned into 0.2 mag intervals. The theoretical expectations, calculated from the optimized differential  $\varphi(M)$  and  $f(m)$  functions, are shown as the curves. The density is assumed to be homogeneous in each velocity interval, but is allowed to vary from interval to interval (i.e., each theoretical curve is normalized to the number of observed galaxies in the bin). Mean  $M_B$  and  $\sigma(M_B)$  values are indicated.

in Figure 8. The fit of the model to the histograms is very good.

It is, of course, clear why  $\langle M \rangle$  becomes fainter as  $v_0$  decreases in a catalog that is apparent-magnitude limited. Faint galaxies are denied inclusion in the catalog at large redshifts. The point is made explicit in Figures 9 and 10, which show the true differential and integral luminosity functions by the solid line, but terminated by the  $f(m)$  completeness function, which begins the termination at different  $M_B$  values for different velocities. Hence the *effective* luminosity function for catalog entries widens as  $v_0$  decreases.

A final comparison of the catalog with the model is shown in Figure 11. The histogram gives the distribution of  $M_B$  for E galaxies alone as the dotted line, and the distribution of E plus S0 as the solid line, using the standard sample at *all* velocities. The solid curve is the predicted distribution, given the optimized  $\varphi(M)$  and  $f(m)$  functions of Table 2, and assuming a homogeneous density function  $D(v_0)$ . In this case the effect of density fluctuations is no longer negligible, and accounts for the structure seen in the histogram. Nevertheless, the predicted function reproduces the real distribution remarkably well.

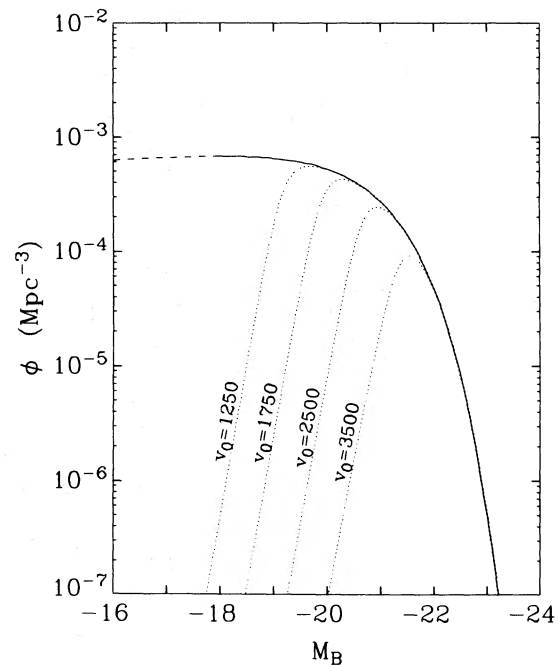


FIG. 9.—Differential luminosity function as the solid line, as cutoff by the completeness function  $f(m)$  that operates in different absolute magnitude ranges for different redshifts. Hence the effective luminosity function widens toward fainter absolute magnitudes as the velocity decreases. This is the reason why  $\langle M_B \rangle$  becomes fainter with decreasing redshift as in Figs. 1, 3, and 8. The total  $\varphi(M)$  is dashed fainter than  $M_B = -18$ , as we have virtually no sensitivity at this level.

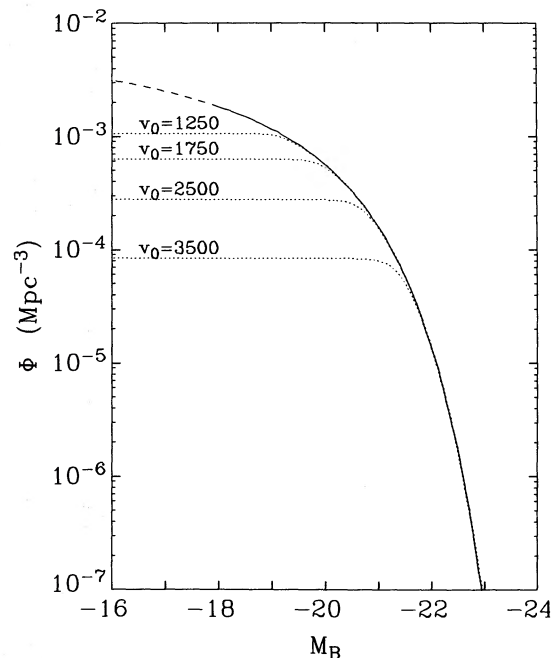


FIG. 10.—Same as Fig. 9, but for the integral luminosity function.

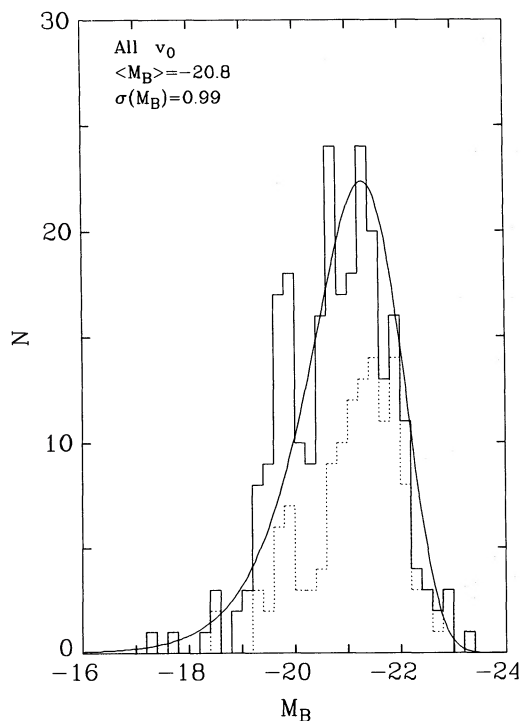


FIG. 11.—Observed (histogram) and predicted (curve) distribution of absolute magnitudes for E and S0 galaxies in the standard sample. The predictions are from the optimized  $\varphi(M)$  and  $f(m)$  functions. Dotted histogram is for E galaxies alone; solid histogram is for E plus S0. Note that the E galaxies are appreciably brighter than the E plus S0 in the mean. Note also the difference between this catalog luminosity distribution and the true differential function of Fig. 9. The difference is caused entirely by the catalog selection effects discussed here.

Note that Figure 11 is the distribution of absolute magnitudes *in the catalog*. A main point of this paper is that this distribution is not at all similar to the true differential luminosity function per unit volume of space as in Figure 5 (or the upper curve of Figure 9) for the reasons discussed in earlier sections.

One final point in Figure 11 is to note that the distribution of  $M_B$  for E galaxies is significantly different from that for E plus S0. The E systems are brighter in the mean by  $\langle \Delta M_B \rangle \approx 0.5$  mag than the combined distribution. This difference is taken into account in Paper III where densities at various distances and in different directions are determined for each Hubble type separately.

## VII. DISCUSSION AND SUMMARY

The purpose of this paper has been to show that the steep relation between mean absolute magnitude and redshift for galaxies in a magnitude-limited catalog is expected when the luminosity function is so broad that faint galaxies are lost to the sample at all redshifts. So stated, the result is obvious, but the consequences are (1) mean photometric distances of galaxies determined by assuming that  $\langle M \rangle$  is not a function of redshift will be systematically in error, (2) distances will be progressively underestimated as redshift increases, and this might naively be interpreted as a systematic deviation from a linear Hubble expansion flow, and (3) the Hubble diagram will not have a mean slope of 5 but will show a much weakened relation between magnitude and redshift.

Objections might, of course, be raised to these points. We have made the analysis by calculating  $M_B$  for individual galaxies in the RSA from a linear velocity field ( $v_0 = Hr$ ), and have derived Figure 1 therefrom. But suppose that, in fact,  $v_0 = H_0 r^3$ , which, as mentioned in § II, would formally give the observed slope of 1.67 to the Hubble diagram (eq. [2]). The methods developed in this paper make it clear that  $v_0 = H_0 r^3$  would not yield a slope of 1.67 in the Hubble diagram *unless the luminosity function were infinitely narrow* (i.e., only if no bias exists in the conversion of apparent magnitude to distance). It follows from the large *observed* width of the luminosity function that if indeed  $v_0 = H_0 r^3$ , then the slope of the Hubble diagram would, in fact, be even smaller than 1.67.

It is to counter any such fallacious identification of the observed slope of the Hubble diagram (formulated with  $v_0$  as the independent variable) with the exponent of the underlying velocity-distance relation that the comparisons between theory and observations have been made in § V. There it was shown that our *required* luminosity and completeness functions agree well with independent observational data (Figs. 5 and 6). Hence we are not making a circular argument by deriving a linear Hubble flow only because such a flow was assumed, because if the underlying flow were not linear, then the derived  $\varphi(M)$  and  $f(m)$  functions would not have agreed with the known external data.

G. A. T. acknowledges support from the Swiss National Science Foundation. A. Y. was supported in part by NSF grant AST 76-80801 A01 at the California Institute of Technology and by RF-UAC Award No. 431-7410A of the State University of New York.

## REFERENCES

- Abell, G. O. 1975, in *Galaxies and the Universe*, ed. A. Sandage, M. Sandage, and J. Kristian (Chicago: University of Chicago Press), chap. 15, p. 601.
- Bahcall, N. A. 1973, *Ap. J.*, **180**, 699.
- Bruzual, A., and Spinrad, H. 1978, *Ap. J.*, **220**, 1.
- Christensen, C. G. 1975, *A. J.*, **80**, 282.
- de Vaucouleurs, G. 1956, *A. J.*, **61**, 430.
- . 1958, *A. J.*, **63**, 253.
- . 1964, *A. J.*, **69**, 737.
- de Vaucouleurs, G. 1966, *Proc. Galileo Conference*, Vol. 2, Tomo 3, ed. L. Rosino (Florence: G. Barbèra), p. 37.
- . 1972, *External Galaxies and Quasi-Stellar Objects*, ed. D. S. Evans (New York: Reidel), p. 353.
- . 1976, *Ap. J.*, **205**, 13.
- de Vaucouleurs, G., de Vaucouleurs, A., and Corwin, W. G. 1976, *Second Reference Catalog of Bright Galaxies* (Austin: University of Texas Press).
- Hawkins, G. S. 1962, *Nature*, **194**, 563.

- Hickson, P. 1977, *Ap. J.*, **217**, 16.  
 Hubble, E. 1936, *Ap. J.*, **84**, 270.  
 Hubble, E., and Humason, M. L. 1931, *Ap. J.*, **74**, 43.  
 Humason, M. L. 1936, *Ap. J.*, **83**, 10.  
 Humason, M. L., Mayall, N. U., and Sandage, A. 1956, *A.J.*, **61**, 97.  
 Jauncey, D. L. 1967, *Nature*, **216**, 877.  
 Kendall, M. G., and Stuart, A. 1973, *The Advanced Theory of Statistics*, Vol. 2 (3rd ed.; New York: Hafner).  
 Malmquist, K. G. 1920, *Medd. Lund Astr. Obs.*, series 2, No. 22.  
 Peebles, P. J. E. 1976, *Ap. J.*, **205**, 318.  
 Rubin, V. C., Thonnard, N., Ford, W. K., and Roberts, M. S. 1976, *A.J.*, **81**, 719.  
 Sandage, A. 1972a, *Ap. J.*, **173**, 485.  
 ———. 1972b, *Ap. J.*, **178**, 1.  
 Sandage, A. 1975, *Ap. J.*, **202**, 563.  
 ———. 1976, *Ap. J.*, **205**, 6.  
 Sandage, A., and Tammann, G. A. 1975, *Ap. J.*, **196**, 313.  
 ———. 1979, *Revised Shapley-Ames Catalog* (Washington, DC: Carnegie Institution of Washington), in preparation (RSA).  
 Sandage, A., Tammann, G. A., and Hardy, E. 1972, *Ap. J.*, **172**, 253.  
 Segal, I. 1975, *Proc. Nat. Acad. Sci.*, **72**, 2473.  
 Schechter, P. 1976, *Ap. J.*, **203**, 297.  
 Silk, J. 1974, *Ap. J.*, **193**, 525.  
 Smoot, G. F., Gorenstein, M. V., and Muller, R. A. 1977, *Phys. Rev. Letters*, **39**, 989.  
 Yahil, A., Tammann, G. A., and Sandage, A. 1977, *Ap. J.*, **217**, 903.

A. SANDAGE: Hale Observatories, Carnegie Institution of Washington, 813 Santa Barbara Street, Pasadena, CA 91101

G. A. TAMMANN: Astronomisches Institut der Universität, Basel, Venusstrasse 7, CH-4102, Binningen, Switzerland

A. YAHIL: Astronomy Program, ESS Building, State University of New York, Stony Brook, NY 11794